

Pacific Sea Surface Temperatures in the Twentieth Century: An Evolution-Centric Analysis of Variability and Trend

BIN GUAN AND SUMANT NIGAM

Department of Atmospheric and Oceanic Science, University of Maryland, College Park, College Park, Maryland

(Manuscript received 4 June 2007, in final form 4 September 2007)

ABSTRACT

A consistent analysis of natural variability and secular trend in Pacific SSTs in the twentieth century is presented. By focusing on spatial *and* temporal recurrence, but without imposition of periodicity constraints, this *single* analysis discriminates between biennial, ENSO, and decadal variabilities, leading to refined evolutionary descriptions, and between these natural variability modes and secular trend, all without advance filtering (and potential aliasing) of the SST record. SST anomalies of all four seasons are analyzed together using the extended-EOF technique.

Canonical ENSO variability is encapsulated in two modes that depict the growth (east-to-west along the equator) and decay (near-simultaneous amplitude loss across the basin) phases. Another interannual mode, energetic in recent decades, is shown linked to the west-to-east SST development seen in post-climate shift ENSOs: the noncanonical ENSO mode. The mode is closely related to Chiang and Vimont's meridional mode, and leads to some reduction in canonical ENSO's oscillatory tendency.

Pacific decadal variability is characterized by two modes: the Pan-Pacific mode has a horseshoe structure with the closed end skirting the North American coast, and a quiescent eastern equatorial Pacific. The mode exhibits surprising connections to the tropical/subtropical Atlantic, with correlations there resembling the Atlantic multidecadal oscillation. The second decadal mode—the North Pacific mode—captures the 1976/77 climate shift and is closer to Mantua's Pacific decadal oscillation. This analysis shows, perhaps for the first time, the striking links of the North Pacific mode to the western tropical Pacific and Indian Ocean SSTs. The physicality of both modes is assessed from correlations with the Pacific biological time series.

Finally, the secular trend is characterized: implicit accommodation of natural variability leads to a non-stationary SST trend, including midcentury cooling. The SST trend is remarkably similar to the global surface air temperature trend. Geographically, a sliver of cooling is found in the central equatorial Pacific in the midst of widespread but nonuniform warming in all basins.

An extensive suite of sensitivity tests, including counts of the number of observational analogs of the modes in test analyses, supports the robustness of this analysis.

1. Introduction

Sea surface temperature (SST) plays a critical role in our planet's climate. Its seasonal distribution as well as departures from the seasonal cycle influence weather and climate in both near and faraway regions. Coherent, large-scale SST departures, or anomalies, are manifest on interannual, decadal, and multidecadal to century-long time scales in the Pacific basin (and other oceans). A particularly well-known and relatively well-

understood anomaly pattern is the El Niño–Southern Oscillation (ENSO), with robust SST variability on interannual time scales in the central and eastern tropical basin, and with ocean–atmosphere interaction as the driving mechanism for the oscillation.

The significance of variability on decadal time scales—commonly referred to as Pacific decadal variability (PDV)—was recognized following the nearly decade-long persistence of anomalous conditions in the extratropical basin since winter of 1976/77 (Nitta and Yamada 1989; Trenberth 1990). The decadal variability of Pacific climate has sometimes been referred to as a “shift” of regime, or just climate shift perhaps, because similar low-frequency changes (including oppositely signed ones) in the earlier twentieth-century record had

Corresponding author address: Sumant Nigam, University of Maryland, College Park, 3419 Computer and Space Sciences Bldg., College Park, MD 20742.
E-mail: nigam@atmos.umd.edu

not been fully appreciated at that time. Pacific decadal variability has received considerable attention since the mid-1990s when ocean climate and fisheries were linked in the North Pacific (Mantua et al. 1997) and when PDV was linked to North American hydroclimate. The warm-season links are apparently important for both seasonal hydroclimate anomalies (e.g., Ting and Wang 1997) and multiyear droughts over the North American continent (e.g., Nigam et al. 1999; Barlow et al. 2001; Schubert et al. 2004; Seager et al. 2005).

The recent signs of climate change have generated substantial interest in separation of natural and anthropogenic variability, necessitating a discriminating analysis of low-frequency variations in the Pacific (and Indian Ocean) basin. The present study addresses this challenge by characterizing the secular trend in Pacific SSTs from an analysis that simultaneously extracts the recurrent spatiotemporal patterns of natural variability. The mutual consistency between natural variability and secular trend characterizations and among the natural variability modes themselves is a defining attribute of this analysis.

The problem is challenging, in part, because high-quality observational records are not of long enough duration for stable characterization of decadal variability and long-term trends in Pacific climate. Besides, some key variables such as subsurface ocean temperature (or heat content), which can effectively track coherent, low-frequency ocean variations, remain inadequately defined. The data challenges notwithstanding, the study describes an innovative analysis of the observations in hand, driven by the premise that a robust, improved characterization of secular trend and natural variability patterns, including PDV structure, is possible with current datasets.

The study presents a *single* analysis for characterization of *all* the nonseasonal modes of Pacific ocean-atmosphere variability, including secular trend. One reason for the lack, hitherto, of a unified analysis concerns the analysis method employed in most previous studies [empirical orthogonal functions (EOFs)], and more specifically, its limitations in discriminating between spatially overlapping patterns having distinct variability time scales. The Pacific, interestingly, is home to at least two such patterns, ENSO and the PDV (e.g., Graham 1994).

The study describes findings on spatiotemporal structure of Pacific SST variability from an analysis that uses spatial *and* temporal recurrence in pattern recognition, all without imposing any periodicity constraints on data—the extended EOF (EEOF) analysis (Weare and Nasstrom 1982). As shown later, rotated EEOF analy-

sis can effectively characterize variability evolution, including nascent phase structure; in contrast, canonical EOF analysis identifies the mature phase, whose large amplitudes contribute most to the explained variance. The present analysis shows how consideration of spatiotemporal recurrence can effectively discriminate between biennial, ENSO, and PDV variability patterns, and between secular trend and natural variability, all without any advance filtering (and potential aliasing) of data.

The primary analysis involving computation of rotated EEOFs of seasonally resolved, unfiltered SST anomalies in the Pan-Pacific domain during the twentieth century (1900–2002) is described in sections 3 and 4, while datasets and the analysis method are briefly discussed in section 2. The stability (robustness) and physicality of variability patterns is ascertained from an extensive suite of sensitivity analysis, reported in sections 4 and 5. A synopsis and concluding remarks follow in section 6.

2. Dataset and analysis method

a. Dataset

The primary data analyzed in this study are the Met Office's (UKMO) Hadley Centre Sea Ice and Sea Surface Temperature dataset (HadISST) 1.1 SST, which is globally available on a $1^\circ \times 1^\circ$ grid for the period from 1870 onward. The SSTs were constructed using a reduced-space optimal interpolation and subsequent insertion of quality-controlled gridded observations onto the reconstruction (Rayner et al. 2003). Because of the relatively long record, data continuity, and statistical homogeneity, HadISST is the dataset of choice for analysis of Pacific low-frequency variability. The National Centers for Environmental Prediction–National Center for Atmospheric Research (NCEP–NCAR) reanalysis (Kalnay et al. 1996) provided the 1000-hPa winds for aspects of the analysis.

Seasonal means are computed from the monthly values, and the seasonal cycle, determined by the long-term mean of each season, is removed. The SST anomalies are interpolated to a $5^\circ \times 2.5^\circ$ longitude–latitude grid in the interest of computational efficiency. To ensure each grid cell's influence in the analysis is commensurate with its area, gridded SSTs were weighted by the square root of the cosine of the latitude (e.g., Chung and Nigam 1999). The SST data were not subjected to additional normalization, in particular, by the local standard deviation. The undertaken EOF analysis is thus covariance rather than correlation based, giving regions with greater variance more influence in deter-

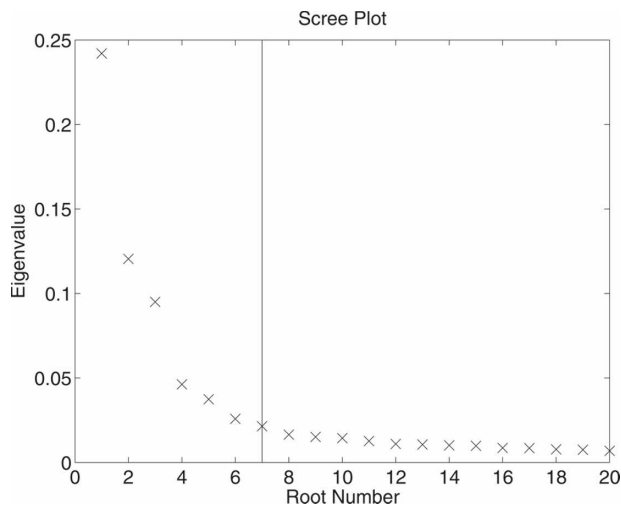


FIG. 1. Scree plot from the rotated extended EOF analysis of Pacific SST variability. The eigenvalues shown are before rotation. The cutoff number for rotation was chosen to be seven, marked by the vertical line.

mining the outcome. The SSTs were also not filtered, as in some previous studies (e.g., Zhang et al. 1997).

The analysis is conducted in the Pan-Pacific domain (20°S – 60°N , 120°E – 60°W), which spans the tropics of both hemispheres and the northern extratropics in the Pacific longitudes. A large domain analysis should yield more accurate characterization of the variability patterns from the full- and not just core-region sampling of patterns. For instance, PDV and ENSO variability can be better defined from sampling of both their tropical and extratropical footprints.

b. Rotated extended EOF

A variant of regular EOF is the so-called extended EOF, which instead of providing a single spatial pattern (a “snapshot” of the mature phase), gives an l -member contiguous sequence of spatial patterns Δt apart in time (Weare and Nasstrom 1982). The parameters l and Δt are chosen so that the focus period ($l\Delta t$) covers a significant portion of variability evolution. The technique is equivalent to multichannel singular spectrum analysis (von Storch and Zwiers 1999) when the chosen pattern interval (Δt) is the same as the sampling interval of the data record. A five-member anomaly sequence at seasonal intervals is used in the primary analysis, and sensitivity to these choices is discussed in section 5.

In canonical EOF analysis, modal structures are selected on the basis of their ability to successively explain maximal variance in the entire analysis domain, which can be both an advantage and a drawback. It would be a drawback if one or more physical modes

TABLE 1. Leading modes identified by the rotated EEOF analysis of unfiltered, seasonal SST anomalies during 1900–2002 in the Pan-Pacific domain of 20°S – 60°N , 120°E – 60°W .

No.	Variance explained (%)	Name	Label
1	17.7	ENSO ⁺	ENSO ⁺
2	13.6	ENSO [−]	ENSO [−]
3	10.2	Trend	Trend
4	5.3	PDV Pan-Pacific	PDV ^{PP}
5	4.3	Noncanonical ENSO	ENSO ^{NC}
6	4.3	PDV North Pacific	PDV ^{NP}
7	3.5	Biennial	Biennial

were dominant only in an analysis subdomain, for their limited contribution to domain variance could then reduce the chances of their correct identification. Not only that, emphasis on maximal accounting of the full domain variance can also make canonical analysis sensitive to domain size. Some of these deficiencies can be remedied by rotation of EOFs (Richman 1986), which yields more stable physical results.

The number of modes rotated in primary analysis is determined by the scree test (Cattell 1966). A “Rule N” test (Overland and Priesendorfer 1982) was first run, which showed the 29 leading EEOFs to be above the noise level. The scree test was conducted by plotting the unrotated eigenvalues against their root numbers, and finding the point where the curve becomes flat. The statistically significant modes to be rotated are those with “large” eigenvalues (i.e., ones easily separable from others in visual inspection of the distribution). For the primary analysis, seven modes are rotated (cf. Fig. 1), and the analysis’s sensitivity to the number of rotated modes is discussed in section 5.

The leading variability modes identified by the primary analysis are described in the next two sections. Seasonal-mean anomalies of all four calendar seasons are analyzed together in the interest of tracking and identifying variability patterns on the basis of recurrent spatiotemporal evolution. The names and labels attached to the modes and the percentage variance they explain are given in Table 1. The corresponding principal components (PCs) are shown in Fig. 2.

3. ENSO evolution

a. Canonical evolution

The current analysis, emphasizing evolution, describes ENSO using two modes, one depicting the growing phase and one its decaying phase; together they describe the canonical ENSO (cf. Rasmusson and Carpenter 1982), as shown in Fig. 3. The season labels

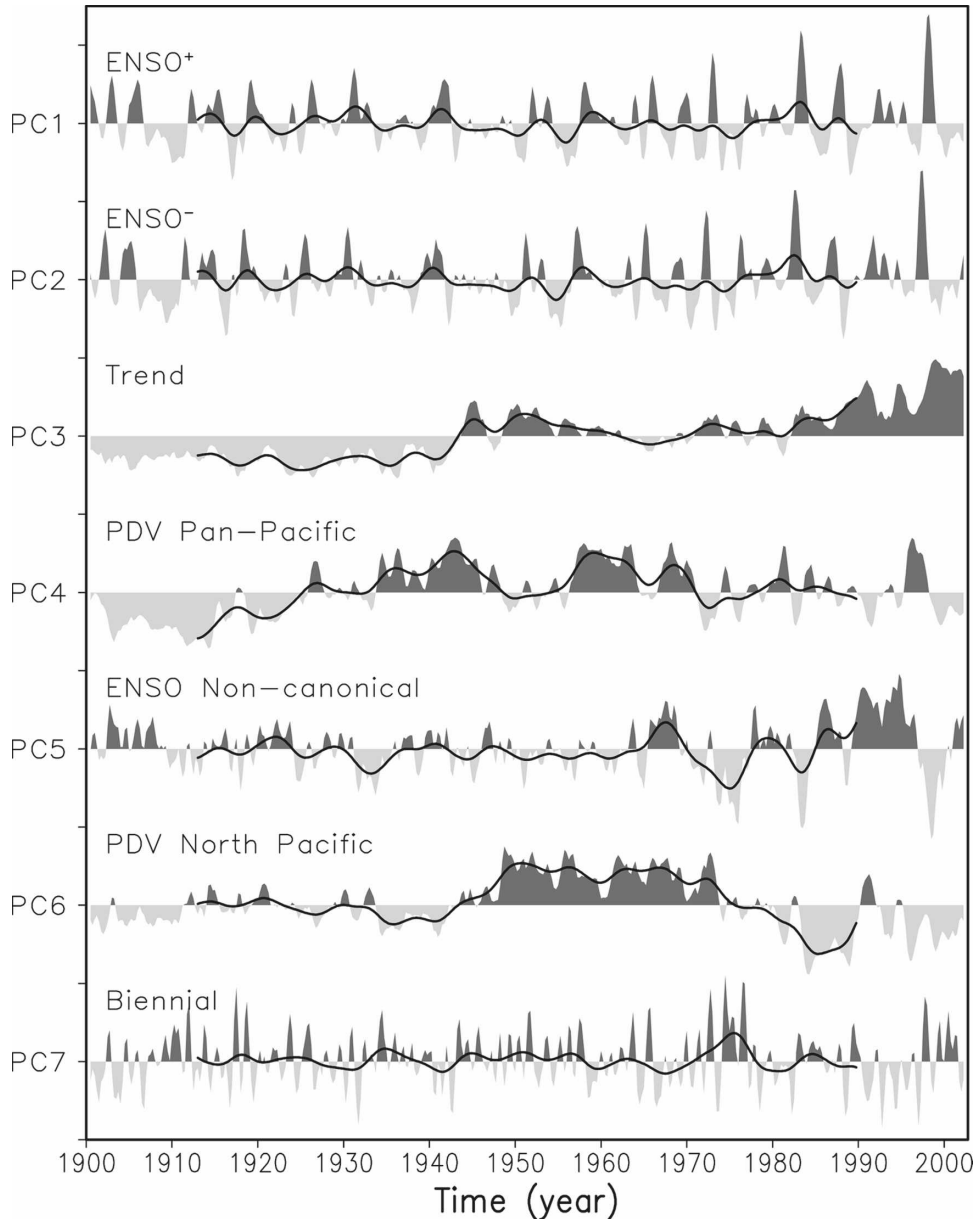


FIG. 2. Leading PCs of Pacific SST variability in the twentieth century (1900–2002). Tick marks on the vertical axis are drawn every three standard deviations. The original PCs are shaded, while heavily smoothed versions (from 50 applications of a 1-2-1 smoother) are shown using solid black lines.

attached to the SST maps in Fig. 3 are obtained from additional analysis,¹ since the primary analysis is an all-season one. Note, ENSO is characterized by its mature phase (northern winter) pattern in regular EOF analysis.

¹ Lead/lag regressions are computed for ENSO PCs, with all but one calendar season's PC zeroed out. Four sets of maps are thus obtained for each ENSO PC. The season labels in Fig. 3 are then determined by finding which of the four maps is closest to the displayed modal evolution.

During the growth phase of ENSO² (hereafter ENSO⁻, “-” for peak minus; Fig. 3, left column), positive SST anomalies first appear in the eastern equatorial Pacific and then extend westward across the date line—the classic evolution. Unlike the growth phase, the decay phase (hereafter ENSO⁺, “+” for peak plus;

² ENSO discussion in the paper is mostly in the context of El Niño evolution, but it is equally applicable to the cold La Niña phase.

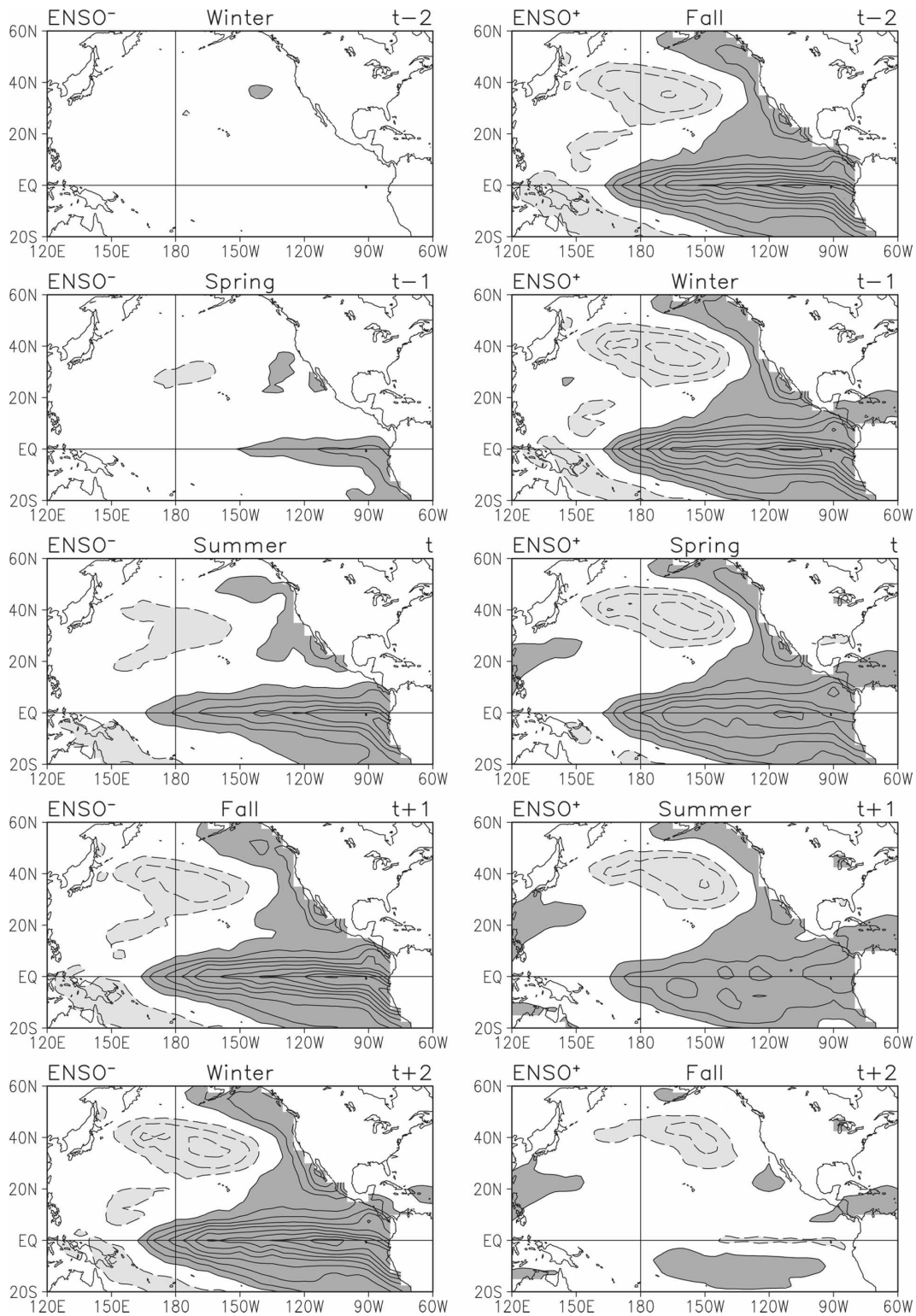


FIG. 3. (left) Canonical ENSO evolution: ENSO⁻ (buildup phase); (right) ENSO⁺ (decay phase). A five-season SST sequence is displayed with time running downward. Maps are assigned calendar seasons based on additional analysis; see text for details. Solid (dashed) contours denote positive (negative) values and the zero contour is suppressed. Contour interval is 0.1 K.

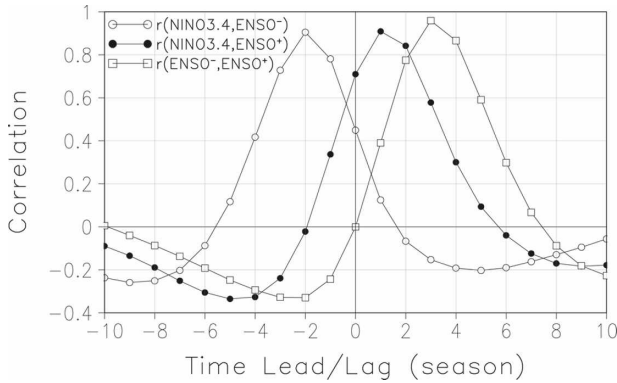


FIG. 4. Cross correlations of ENSO⁻ and ENSO⁺ PCs, and of each with the Niño-3.4 SST index, at various seasonal leads/lags. The curve key is in the upper left corner, with the following plotting convention: when $r(A, B) > 0$ for $t < 0$, B leads A ; if $r > 0$ for $t > 0$, B lags A . Cross correlations show that ENSO⁻ (ENSO⁺) PC leads (lags) the Niño-3.4 index by two (one) seasons, and consistently, ENSO⁺ lags ENSO⁻ by three seasons.

Fig. 3, right column) is characterized by near-simultaneous loss of amplitude across the basin, the loss being especially steep during spring and summer. The rapid summer-to-winter buildup and the slow winter-to-summer demise of the midlatitude basin anomalies are also noteworthy. Although not investigated here, there is indication of SST development in the tropical North Atlantic and western Pacific (and Indian Ocean, not shown) with ENSO maturity and decay, consistent with earlier findings [e.g., Carton and Huang (1994) on the Atlantic and Nigam and Shen (1993) on Indian Ocean links].

The relation between ENSO PCs and the Niño-3.4 SST index (a widely used marker of ENSO variability) is shown in Fig. 4. The ENSO⁻ (ENSO⁺) PC leads (lags) the Niño-3.4 index by two (one) seasons, consistent with the spatial patterns in Fig. 3, in that simultaneous regressions of the ENSO⁻ (ENSO⁺) PC represent the summer (spring) season pattern. The PCs themselves have a three-season shift in time.

b. Noncanonical evolution

Of special interest is the fifth-leading mode, the most notable feature of which is *eastward* development of positive SST anomalies along the equator, beginning with the central Pacific ones (Fig. 5). As this development is opposite of that in canonical ENSO, the mode is referred to as the noncanonical ENSO mode (labeled

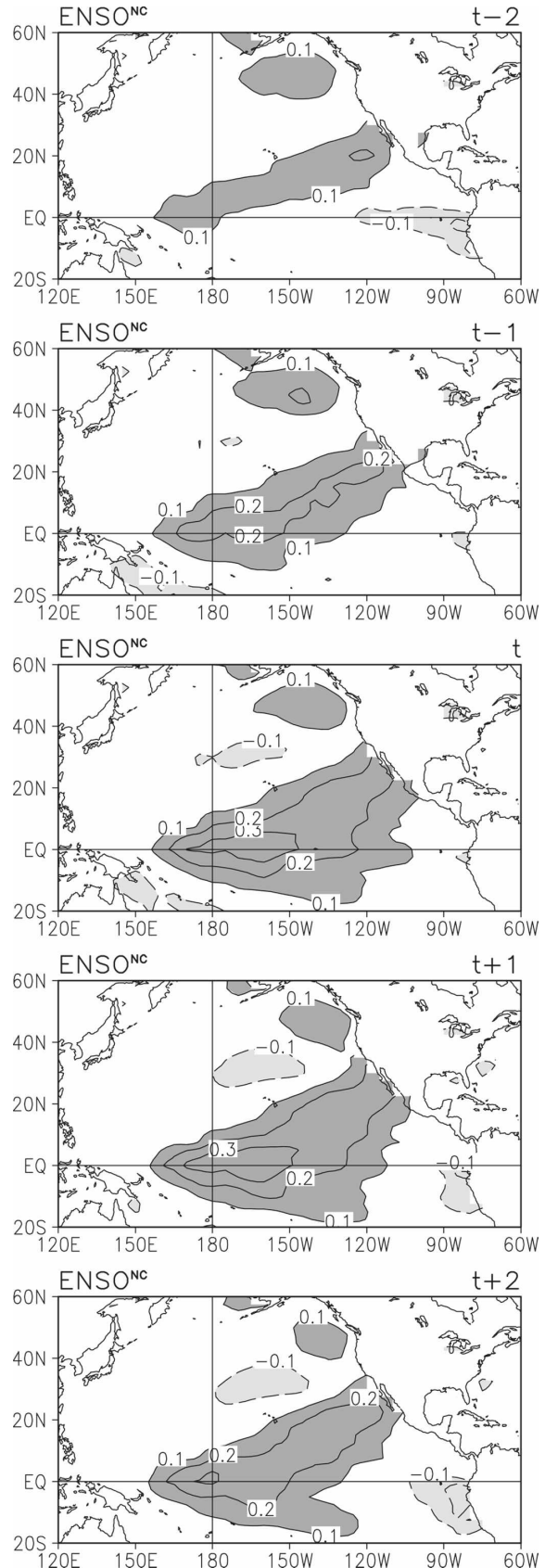


FIG. 5. Noncanonical ENSO evolution over a five-season span, with time running downward. Contour/shading convention is as in Fig. 3.

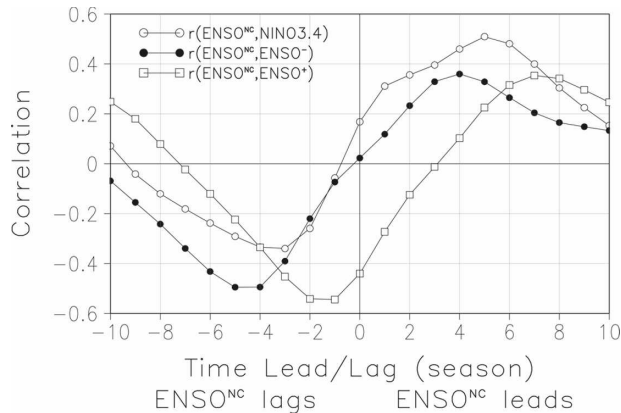


FIG. 6. Cross correlations of the noncanonical ENSO mode (ENSO^{NC}) with ENSO^- and ENSO^+ PCs and the Niño-3.4 SST index; all in the 1977–2002 subperiod when ENSO^{NC} is particularly energetic. The curve key is in the upper left corner and the plotting convention is the same as in Fig. 4; also indicated along the x axis here. The cross correlations show $\text{ENSO}^-/\text{Niño-3.4}/\text{ENSO}^+$ to lag ENSO^{NC} by 4/5/7 seasons.

ENSO^{NC}). A striking feature of the mode is also its connection to the North American continent, which intensifies with equatorial SST development. The northeastward sloping SST structure is reminiscent of the northeast trade wind distribution, and not inconsistent with diminished trade winds and latent heat flux.

The ENSO^{NC} PC exhibits stronger amplitude and longer time scales in the post-climate shift (1977 onward) period (cf. Fig. 2). Correlations with the Niño-3.4 index are strongest at a five-season lead in the recent period (see Fig. 6, open circles), and contemporaneously in the earlier period (not shown). The mode thus opposes canonical ENSO evolution in the 1977–2002 period. Given that El Niño SST anomalies exhibit west-to-east development in this period (Wang 1995), the ENSO^{NC} mode must not only oppose but overwhelm the canonical mode contributions, at least in this feature. Equatorial SST development can be surmised from the Fig. 6 cross correlations.³

The ENSO^{NC} mode captures recent changes in ENSO evolution. The progressively increasing variance and period manifest in this mode's PC in recent decades are consistent with previous findings on increased ENSO energy and persistence in the post-climate shift period (e.g., Gu and Philander 1995; Zhang and Busa-

³ The negative correlation (-0.54) between ENSO^{NC} and ENSO^+ modes at -1 season indicates that the former lags the negative phase of the latter (i.e., the ENSO^{NC} follows La Niña decay). The positive correlation (0.36) between the noncanonical and ENSO^- modes at $+4$ seasons, on the other hand, indicates that coastal warming follows the ENSO^{NC} mode (or central Pacific SST development), by almost a year.

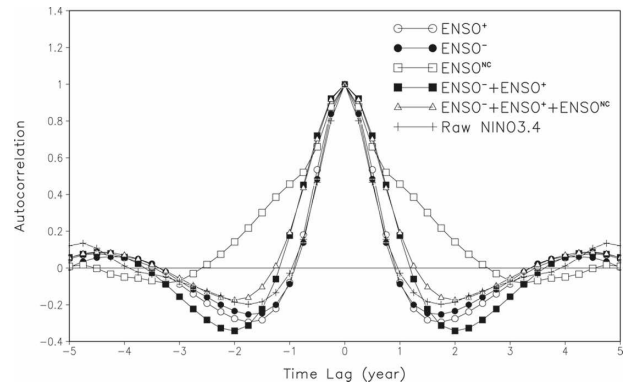


FIG. 7. Autocorrelation of the ENSO^- , ENSO^+ , and ENSO^{NC} PCs, and the original and synthetic Niño-3.4 SST indices. Synthetic indices are from SST reconstruction using various combinations of ENSO modes; the curve key is in the upper right corner.

lacchi 2005). Using nonlinear, neural network-based EOF analysis, Monahan (2001) found a noncanonical ENSO mode that also characterized temporal nonstationarity relatable to the 1976/77 climate shift; spatial evolution of this mode, however, differs from the one described herein. ENSO-unrelated interannual SST variability was also investigated by Mestas-Nuñez and Enfield (2001), and their 0–8-yr mode could well represent aspects of noncanonical ENSO (and biennial, discussed later) variability. Departures from canonical El Niño development have been also characterized using the Trans-Niño index (Trenberth and Stepaniak 2001), which is defined as the difference between the normalized SST anomalies in the Niño-1 + -2 and Niño-4 regions. This index is correlated with ENSO^{NC} PC at -0.65 .

c. Evolution time scale

The inherent time scale of canonical and noncanonical ENSO modes is estimated from lead/lag autocorrelations of their PCs (Fig. 7). Also shown are autocorrelations of the original and synthetic Niño-3.4 SST indices. The original index is the standard one (i.e., from “raw” SST anomalies) while synthetic ones are from reconstructed SST anomalies. Anomalies are reconstructed from canonical and noncanonical PCs by adding products of PCs and their zero-lag regressions. Synthetic Niño-3.4 indices are then generated in the usual manner, by averaging SST anomalies in the 170° – 120°W and 5°S – 5°N equatorial strip.

The lead/lag autocorrelation statistic is a simple, straightforward way to analyze event longevity and identify oscillatory time scales. The width of the autocorrelation curve provides an estimate of event duration in any one phase, or the approximate half-period.

Inspection of Fig. 7 shows the canonical modes (ENSO^- , ENSO^+) and the standard Niño-3.4 index to have similar distributions, with first zero crossings at ± 1 yr (i.e., about 2 yr apart). In contrast, autocorrelations of the ENSO^{NC} PC fall off more slowly, leading to first zero crossings that are 5–6 yr apart. Interestingly, these longer time scales are not prominently manifest in the synthetic Niño-3.4 index ($\text{ENSO}^- + \text{ENSO}^+ + \text{ENSO}^{\text{NC}}$), reflecting dominance of the canonical contributions. The addition of ENSO^{NC} mode to canonical variability does, however, reduce autocorrelations of the derived index at ± 2 yr, from -0.34 to -0.17 , leading to reduced oscillatory tendency. Given that ENSO^{NC} mode is notably flexed in recent decades, one would expect ENSO phase transitions in the earlier period to be more regular, assuming other modes are, energetically, quasi-stationary. Perusal of PCs in Fig. 2 indicates this is not the case, perhaps, because of significant variations in the energy of the canonical modes themselves.⁴

The difference in autocorrelation distribution of the standard and synthetic Niño-3.4 indices, especially in zero crossing times, is also noteworthy in Fig. 7. Zero crossings of both synthetic indices are further apart by ~ 0.5 yr, pointing to a somewhat longer ENSO period than indicated by the standard index. As the three-mode synthetic index is based on all ENSO-related modes in the EEOF analysis, the period discrepancy is a bit perplexing, leading one to question the suitability of the standard Niño-3.4 SST index as a marker of true ENSO variability (defined by the three-mode synthetic index, in context of this analysis).

Alternatively, one could ask if this difference in ENSO period can be accounted for by inclusion of the only other, and hitherto unconsidered, interannual mode—biennial variability (shown and discussed later)—in the synthetic index definition. The expanded four-mode definition, indeed, eliminates the above-noted difference in autocorrelation functions. While this is reassuring, it does emphasize the implicit inclusion of biennial variability in the standard Niño-3.4 index. For reference, seasonal correlations of the standard Niño-3.4 SST index with synthetic indices in the 1900–2002 period are 0.84 with the two-mode (canonical modes) index, 0.92 with the three-mode (additional ENSO^{NC}) index, and 0.95 with the four-mode (additional biennial) index.

⁴ Increased energy of the canonical modes in the post-climate shift period is reflected in greater negative autocorrelations of the related synthetic Niño-3.4 index at 2-yr lead/lag: -0.52 versus -0.29 in the earlier period and -0.34 in the full record.

d. SST evolution at the equator

ENSO evolution is commonly described by displaying SST development at the equator. The Hovmöller display is helpful in tracking the longitudinal propagation of SST anomalies and in monitoring ENSO period. Evolution is examined through lead/lag index regressions in the entire record and in the pre- and post-climate shift periods. Figure 8 shows equatorial SST evolution over a nine-season span centered on the ENSO warm phase. Regressions of the standard Niño-3.4 SST index based on the full twentieth-century record are shown in the top left panel, while those for the pre- and post-climate shift periods are in the top middle and top right panels. Immediately apparent is the very different evolution of equatorial SST anomalies: from east-to-west in the earlier record (canonical picture) and west-to-east in recent decades (noncanonical development), with the full-period regressions being a weighted average.

The contribution of canonical modes (ENSO^- and ENSO^+) in equatorial SST development, from regressions of the related synthetic Niño-3.4 index, is displayed in the second from top row. There is evidently little change in evolution structure across periods other than an amplitude increase in recent decades. The canonical contribution is thus quite stationary with respect to climate shift and at odds with the recent evolution, not surprisingly. The combined contribution of the canonical and noncanonical modes is plotted in the second from bottom row for all three periods, again from regressions of a synthetic index but one based on three modes. It is apparent that only when ENSO^{NC} is included in the reconstruction can the change in SST evolution across the climate shift be reproduced. The century-based pattern is also in better accord, with maximum amplitudes being more away from the South American coast.

Consideration of canonical and noncanonical modes has led to credible reconstruction of ENSO SST evolution at the equator, but not in one aspect—the duration of warm anomalies, which is shorter in regressions of the standard Niño-3.4 index (top row). The implicit inclusion of biennial variability in the standard index must lead to this discrepancy, for reasons noted earlier (cf. Fig. 7). This is verified from yet another construction of SST evolution (bottom row), this time from regressions of the four mode-based Niño-3.4 index, the fourth mode being biennial variability. The new reconstruction is in remarkable agreement with that displayed in the top row, confirming the significant but implicit contribution of biennial variability in the standard Niño-3.4 SST index.

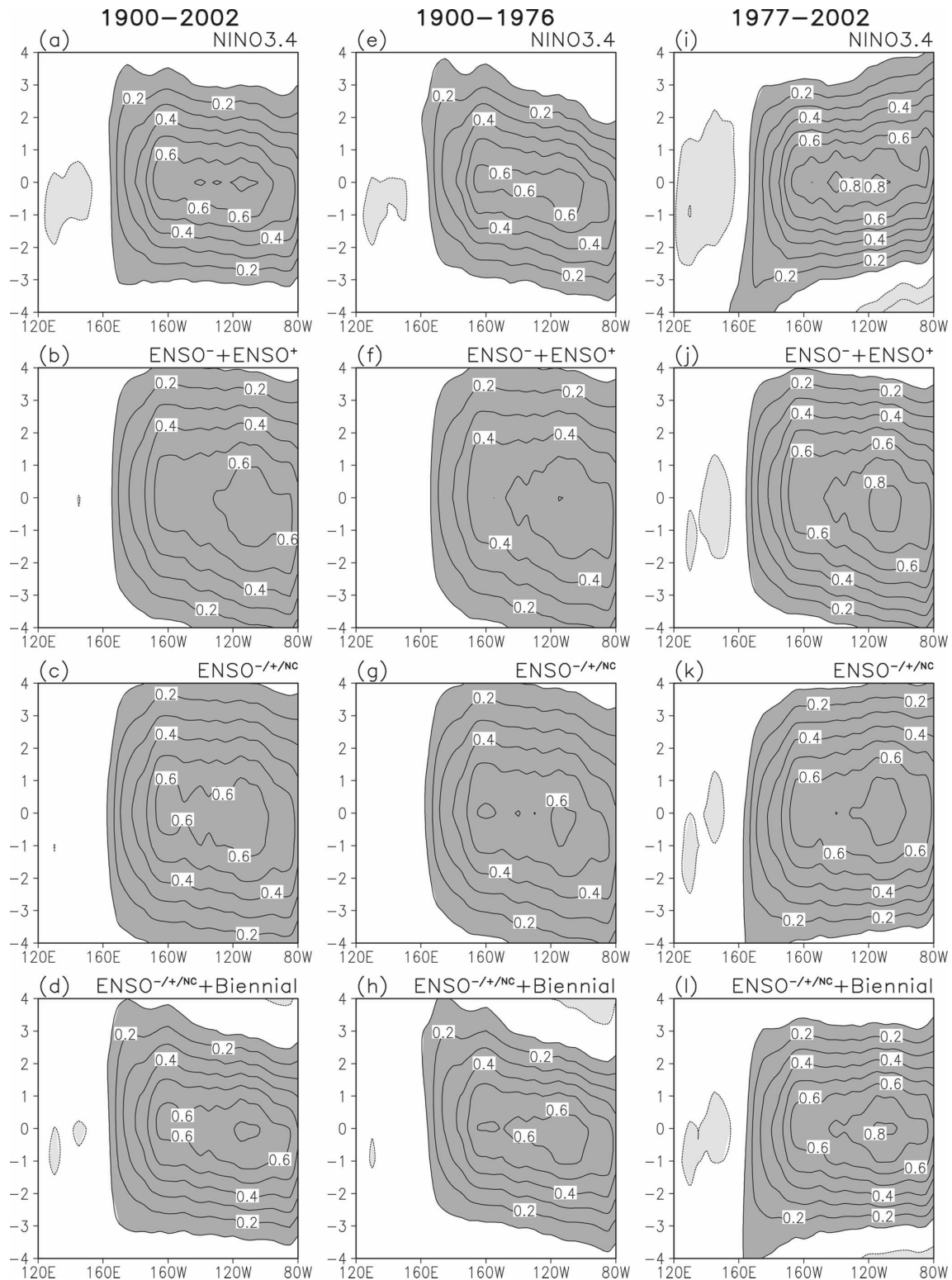


FIG. 8. ENSO SST evolution at the equator: lead/lag regressions of the Niño-3.4 SST index, with time running upward. The 5°S – 5°N averaged SSTs are displayed over a nine-season span. Regressions of synthetic and (a), (e), (i) original indices are shown. Synthetic index is from the (b), (f), (j) two canonical modes, (c), (g), (k) canonical + noncanonical, and (d), (h), (l) canonical + noncanonical + biennial modes, as also indicated in the title line of each panel. Three time periods are examined: (left) 1900–2002 (full period), (middle) 1900–76 (pre-climate shift), and (right) 1977–2002 (post-climate shift). Contour/shading convention is as in Fig. 3.

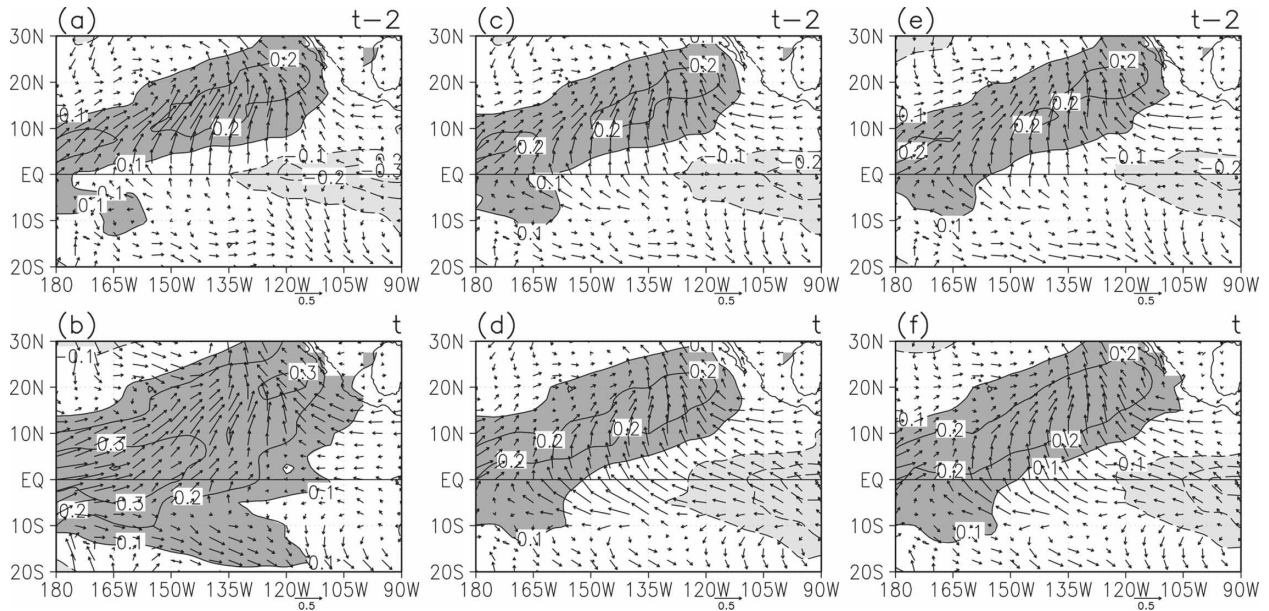


FIG. 9. SST and 1000-hPa wind regressions of the ENSO^{NC} mode in the 1949–2002 period: the (a), (c), (e) two-season lead and (b), (d), (f) simultaneous regressions are displayed. The ENSO^{NC} PC is from the primary 1900–2002 period analysis in (a)–(d), and from the rotated EEOF analysis of detrended 1945–2002 SSTs in (e), (f) [to facilitate comparison with Chiang and Vimont (2004)]. Regressions in (c)–(f) are on detrended and ENSO-filtered fields; see text for more details. Contour/shading convention is as in Fig. 3.

The earlier posed question on which ENSO index—standard or the three mode-based synthetic Niño-3.4 SST index—better marks ENSO variability is now weightier, especially in context of theoretical and modeling analysis of ENSO dynamics and thermodynamics.

e. ENSO^{NC} and Pacific meridional mode

Recently, Chiang and Vimont (2004) have argued for the existence of a meridional mode in the Pacific basin, similar to the one posited for the Atlantic where the mode represents interannual-to-decadal variability in the tropical basin. Both meridional modes are envisioned to be similarly driven, through SST–wind coupling in the deep Tropics and wind-driven SST anomalies in the northern Tropics. The meridional mode is the leading mode in Chiang and Vimont’s maximum covariance analysis of Pacific SST and 10-m wind, but after the local linear trend and ENSO variability is removed from the data. ENSO variability is filtered by subtracting regressions of the Pacific cold tongue index⁵ (CTI; Deser and Wallace 1990).

⁵ The SST cold tongue index, defined as the average SST anomaly in the 6°S–6°N, 180°–90°W equatorial box, is also commonly used to mark ENSO variability. Its seasonal correlation with the Niño-3.4 SST index is 0.99 in the 1900–2002 record.

Our interest in investigating links between the meridional and ENSO^{NC} modes stems from their common characterization as being independent of ENSO variability: in a linear sense in the case of the meridional mode, and in a modal context in the case of ENSO^{NC}. Despite linear/modal independence, these modes remain connected to aspects of ENSO variability: ENSO nonlinearity in case of meridional mode, and noncanonical evolution in case of the ENSO^{NC} mode. Such common attributes motivate the present examination of sameness of these modes.

The SST and 1000-hPa wind regressions of the ENSO^{NC} PC are plotted in Figs. 9a,b in a domain and format similar to Chiang and Vimont’s (2004) Fig. 1a and with their analysis period (second half of the twentieth century); ENSO^{NC} PC is still from the earlier, full-period analysis. The SST pattern, especially the one at two-season lead (Fig. 9a) is similar to Chiang and Vimont’s in the tropics and subtropics, but wind features along the equator are less similar. The simultaneous pattern (Fig. 9b) exhibits even less similarity in view of SST development at the equator in the intervening season. The lack of correspondence likely results from how data is filtered in the two analyses. Chiang and Vimont prefilter the data, as described above, and while there is no explicit filtering here, temporally orthogonal PCs in EOF (and EEOF) analysis

effectively filter the record for unrelated variability.⁶ But there is no assurance that the same signal is getting filtered in both analyses, especially since the standard Niño-3.4 SST (or cold tongue) index also represents aspects of ENSO^{NC} and biennial variability, as shown earlier in this section.

The ENSO^{NC} structure is thus reexamined in Figs. 9c,d, this time from PC regressions on explicitly filtered SST, with the filtering exactly as in Chiang and Vimont. The PC is from the primary (full twentieth century) analysis, as before, given our interest in robust characterization of the secular trend in context of natural variability. The regressions, especially the simultaneous one (Fig. 9d), now exhibit a striking correspondence with the Chiang and Vimont (2004) SST and wind patterns. Further and more conclusive support for the sameness of the meridional and ENSO^{NC} modes comes from rotated EEOF analysis of the detrended 1945–2002 SSTs. Regressions of the ENSO^{NC} PC from this analysis,⁷ shown in Figs. 9e,f, are almost indistinguishable from patterns in Figs. 9c,d and also from Chiang and Vimont's Fig. 1a.

The above analysis shows that the ENSO^{NC} mode is closely related to the meridional mode of Chiang and Vimont (2004). It moreover suggests that the largely tropical ENSO^{NC} mode, while not involved in canonical ENSO evolution, encapsulates lower-frequency changes in ENSO variability, as shown in Figs. 6–8. Its seasonal structure and evolution must therefore be characterized in the context of *all* nonseasonal modes of variability with tropical footprints (canonical ENSO, biennial, decadal variability, and climate trend), much as in this study. The analysis also highlights the pitfalls of using the standard Niño-3.4 (or cold tongue) SST index to represent (filter) canonical ENSO variability.

f. Biennial variability

Biennial variability is captured by the seventh (last) mode; see structure of PC7 in Fig. 2. Biennial variability in the tropical Pacific was noted in context of ENSO variability by Rasmusson et al. (1990), who argued for its importance in the ENSO cycle on the basis of the near 2-yr time scale of individual warm and cold events and their phase locking with the annual cycle. Rasmusson et al. viewed ENSO as a superposition of biennial and lower-frequency variability—a view strongly supported by our analysis of SST evolution especially (see Figs. 7–8).

The biennial mode (Fig. 10) shows SST anomalies

emerging from the eastern equatorial Pacific and extending westward over time, toward the date line. At the beginning of the displayed cycle, SSTs resemble the cold ENSO phase. However, in just about three seasons ($t-3$ to t), SSTs switch sign and become tightly focused around the equator in the central/eastern basin. The amplitude (≤ 0.4 K) and meridional extent are also smaller than in canonical ENSO. This biennial variability structure is somewhat different from earlier descriptions: the asymmetry in cold and warm phase evolutions and westward propagation of SSTs in the cold tongue sector were, perhaps, not recognized earlier. Pacific biennial variability also had links to the Indian Ocean in Rasmusson et al. (1990) and Barnett (1991), but none are evident here.

4. Pacific decadal variability and secular trend

Decadal variability is captured by two modes in this analysis: the fourth (Pan Pacific) and the sixth (North Pacific) leading modes. The related PCs (Fig. 2) exhibit variations on long time scales (longer than ENSO's), capturing the climate shifts in the twentieth century: PC4 has the 1920s shift, while the shifts from the 1940s and mid-1970s are manifest in PC6. These shifts have been noted in the context of Pacific SST variability by Mantua et al. (1997) and Minobe (1997).

a. Pan-Pacific mode

The Pan-Pacific (hereafter PDV^{PP}) evolution is shown in Fig. 11, with panels now a year apart; regressions in the analysis domain are on the lhs, while global SST correlations are on the rhs. The PDV^{PP} mature phase (second panel from the bottom) contains negative SST anomalies in a limited region of the central North Pacific, surrounded by stronger positive anomalies extending eastward from the Bering Sea and then downward until Baja California, and then sweeping back southwestward toward the tropical Pacific (a horseshoe-shaped structure). Noteworthy is the lack of SST anomalies in the central/eastern equatorial Pacific and hints of clockwise development along the North American west coast, with SSTs becoming as large as 0.4 K before decaying.

A Pan-Pacific mode equivalent has been identified in some previous studies, but with somewhat different structure and names. Our PDV^{PP} is similar to Barlow et al.'s (2001) where data were not prefiltered and rotation applied, as here, but where regular rather than EEOF analysis was executed. Barlow et al.'s mode (their Fig. 2b) exhibits a far greater equatorial reach than ours though. Our PDV^{PP} structure differs from Zhang et al. (1997), Nakamura et al. (1997), and Wu et al. (2003) notably in the quiescence of the central/

⁶ PC orthogonality remains intact under EOF rotation.

⁷ The new ENSO^{NC} PC is correlated at 0.95 with the original one (cf. Fig. 2) in the overlapping period.

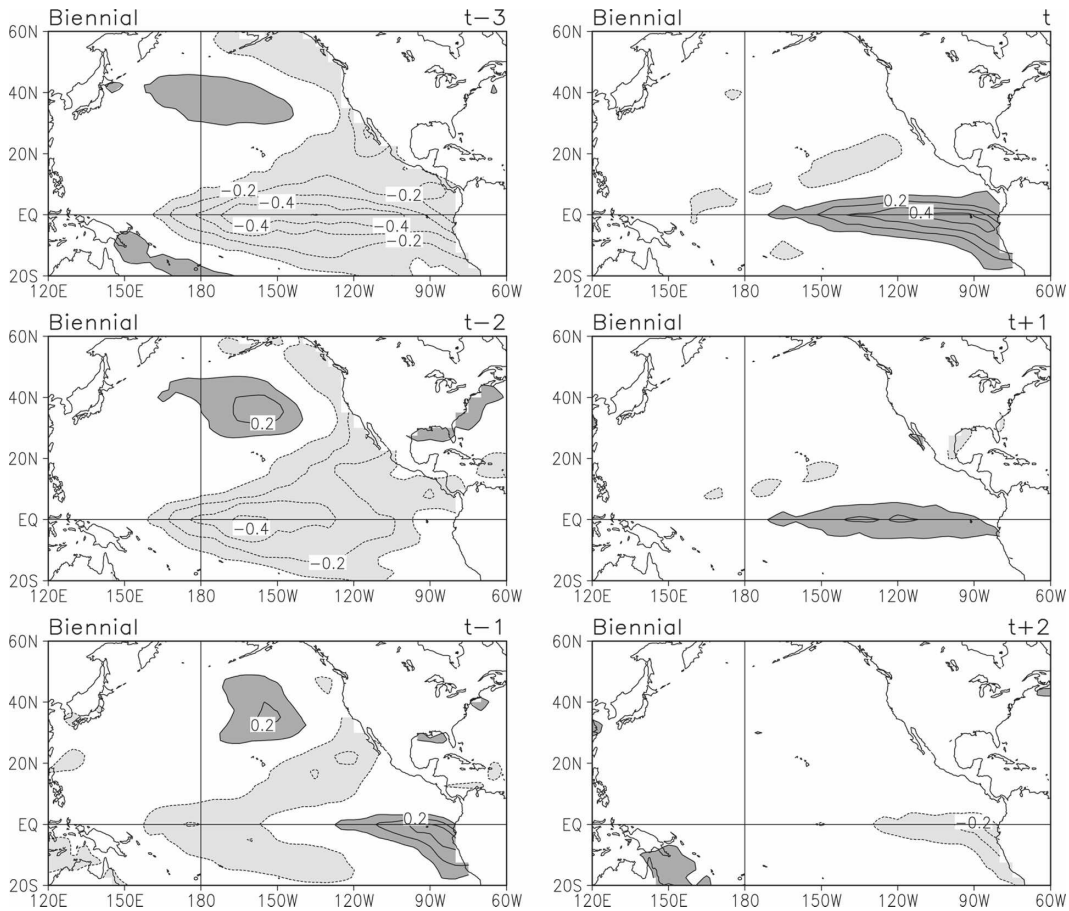


FIG. 10. Biennial variability evolution over a six-season span, with time running downward in both columns. Contour/shading convention is as in Fig. 3.

eastern equatorial Pacific in all phases, and in the near insignificance of SST anomalies in the central North Pacific. This mode has been referred to as “ENSO-like” (e.g., Zhang et al. 1997), a somewhat misleading name in our opinion, given the very different spatiotemporal structure of ENSO (Fig. 3) and PDV^{PP} (Fig. 11). [For reference, the Pan-Pacific mode and Mantua et al.’s Pacific decadal oscillation (PDO) are correlated at 0.23; this is not surprising, given the PDO’s North Pacific focus.]

The origin of Pacific decadal variability remains intriguing, but global SST correlations of the PDV^{PP} mode provide some insights; correlations are contoured at 0.1 intervals, beginning with 0.2 on the rhs of Fig. 11. Immediately apparent is the strong connection to the northern Atlantic, especially the western tropical/subtropical basin, a weak link to the equatorial Pacific, particularly in the premature phase, little connection to the central North Pacific sector, and the development of an Indian Ocean connection (albeit modest) during modal evolution.

The PDV^{PP} links with the Atlantic, especially the

Caribbean where correlations are $\sim 0.4\text{--}0.5$, indicate Pacific–Atlantic basin connectivity on decadal time scales. While such connections have not been explicitly analyzed, they are to an extent manifest in the analysis of Mestas-Nuñez and Enfield (1999, their rotated EOF 1 and 2) and in the related Atlantic multidecadal oscillation (AMO) SST footprint (Enfield et al. 2001, their Fig. 1b). An intercomparison shows considerable similarity between the PDV^{PP} mature phase footprint in the Atlantic and the AMO structure. The modes are also temporally linked: seasonal correlation is 0.42, and 0.48 with the PDV^{PP} leading AMO by five seasons. To be sure, there are differences between these modes as well, in part due to differences in the underlying analyses (e.g., Mestas-Nuñez and Enfield detrended and prefiltered SSTs prior to analysis, based on complex EOFs; their analysis period was also different).

b. North Pacific mode

The second decadal mode (North Pacific, hereafter PDV^{NP} ; Fig. 12, lhs) is characterized by a zonally elon-

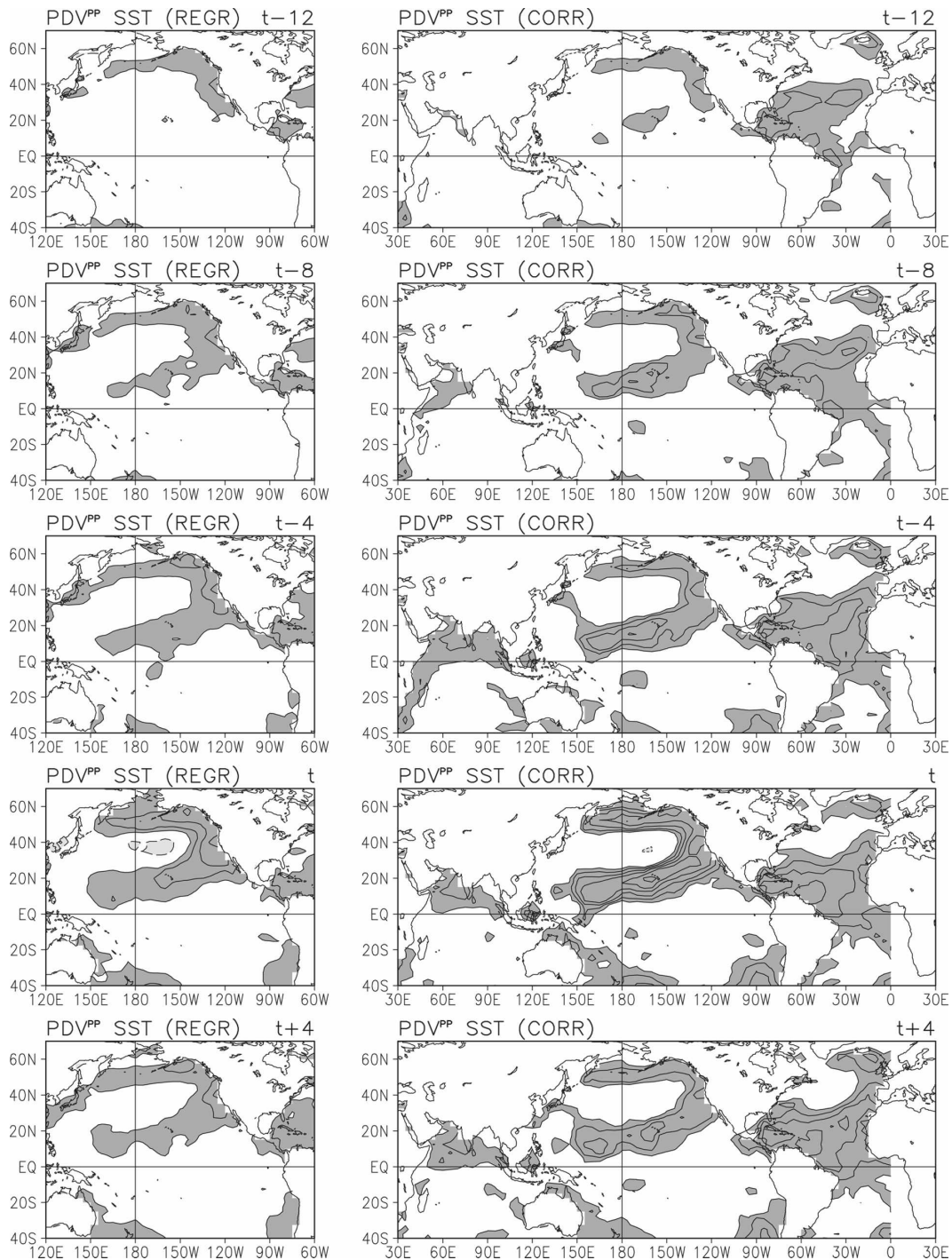


FIG. 11. Evolution of Pan-Pacific decadal SST variability (PDV^{PP}): (left) Pacific basin regressions and (right) global correlations are shown over a 5-yr span, at yearly intervals. Contour interval and shading threshold is 0.1 K in left panels. Correlations are also contoured at 0.1 intervals, but the contouring and shading threshold is 0.2. The remaining is as in Fig. 3.

gated band of positive SST anomalies centered along the sub-Arctic front and the date line. Modal evolution apparently involves tropical SSTs as well: cold SST development in the eastern basin in tandem with the

growth of positive anomalies in the central North Pacific. A causal role for eastern Pacific SSTs is, however, unlikely given their modest amplitude (≤ 0.2 K) and location (atop the climatological SST cold tongue). SST

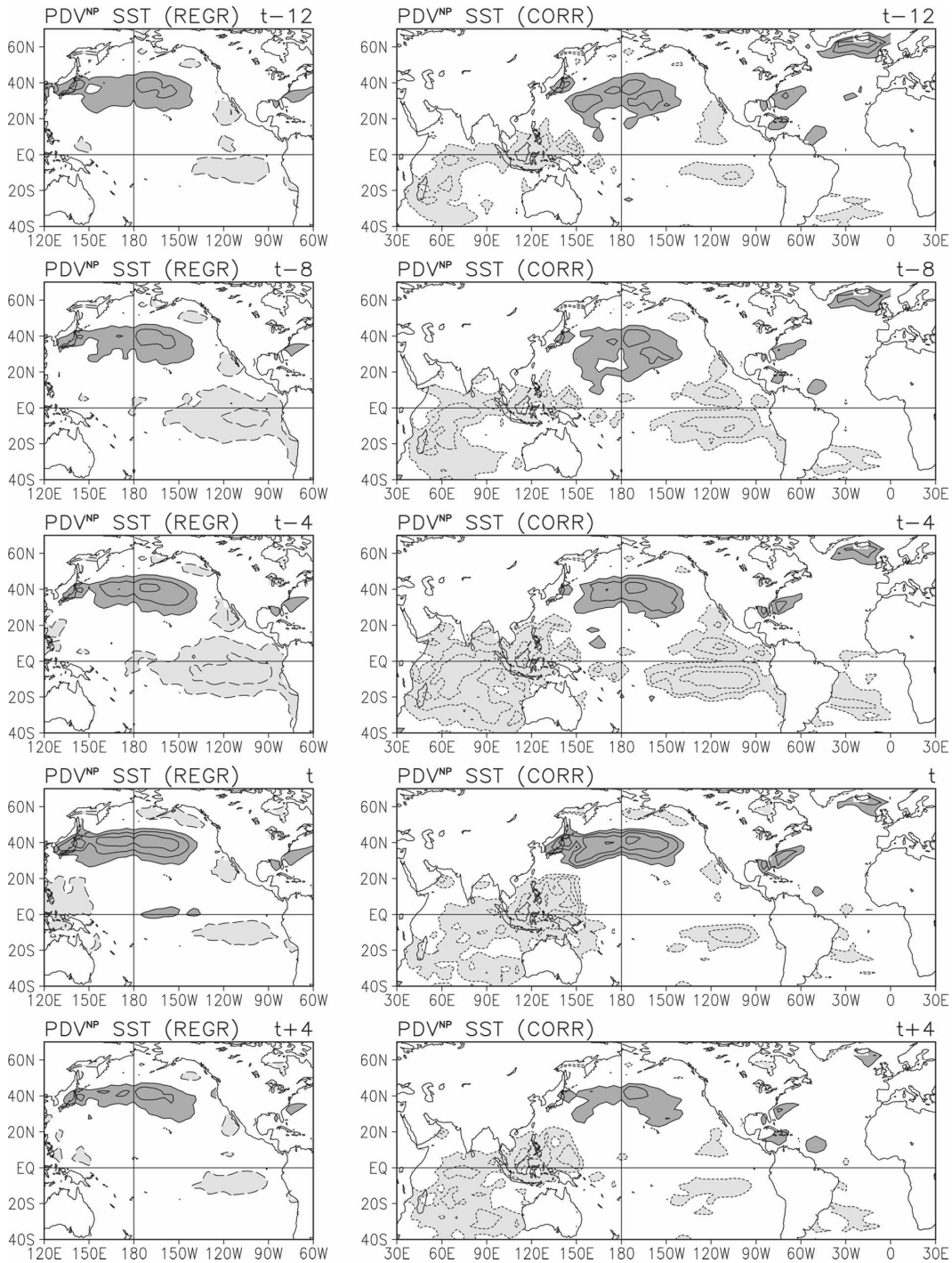


FIG. 12. Evolution of North Pacific decadal SST variability (PDV^{NP}) over a 5-yr span; remaining as in Fig. 11.

anomalies are even weaker in the Indian Ocean and the western tropical Pacific but potentially more significant (see rhs of Fig. 12), given the smaller SST interannual variability there, and more influential given the much warmer climatological state on which they reside. Note, the tropical Indian Ocean was recently shown to be a

sensitive forcing region for the North Pacific climate (Deser and Phillips 2006).

A distinct North Pacific mode of decadal variability, similar to PDV^{NP} , was noted in earlier studies (e.g., Deser and Blackmon 1995; Nakamura et al. 1997; Mantua et al. 1997; Nigam et al. 1999; Barlow et al. 2001; Wu

TABLE 2. Correlations of the two PDV principal components with selected biological time series in the data available period (1965–97). Time series 1–3, 4–6, and 7–9, in the Hare and Mantua (2000) dataset, are most correlated with the PDV^{PP}, PDV^{NP}, and PDO index, respectively. All time series are annually resolved. The numbers following the time series name are the original dataset tags, listed for reference here. Note, time series 4 and 7 are identical.

No.	Biological time series	PDV ^{PP}	PDV ^{NP}	PDO
1	Eastern Pacific zooplankton biomass (40)	0.54		0.10
2	British Columbia coho salmon catch (67)	−0.42		−0.17
3	British Columbia pink salmon catch (68)	−0.42		−0.13
4	Gulf of Alaska halibut recruitment (43)		−0.74	0.73
5	West Coast mackerel recruitment (81)		−0.73	0.66
6	Central Alaska chinook catch (51)		−0.68	0.59
7	Gulf of Alaska halibut recruitment (43)	−0.13	−0.74	0.73
8	Eastern Bering Sea rock sole recruitment (20)	0.24	−0.61	0.67
9	Central Alaska pink catch (54)	0.29	−0.62	0.67

et al. 2003). Because of the North Pacific focus, Mantua's PDO and our PDV^{NP} resemble each other in the midlatitude basin (the two are correlated at -0.57); both capture the recent 1976/77 climate shift as well. Not all previous extractions of the North Pacific mode share this attribute though (e.g., Deser and Blackmon).

The origin of North Pacific decadal variability remains to be elucidated. The shortness of the observational record has stymied progress, as also the finding of weak connections to the tropical Pacific in context of a mindset (based on two decades of ENSO research) reflecting the primacy of the tropics.

The rhs of Fig. 12 displays global SST correlations of the PDV^{NP} PC, and shows, perhaps for the first time, rather striking links of the North Pacific decadal mode to the western tropical Pacific and Indian Ocean SSTs—links not evident in the regression patterns for reasons noted earlier. The western Pacific/Indian Ocean correlations develop in tandem with the opposite signed ones in the North Pacific: being ~ 0.3 at $t - 8$, ~ 0.4 at $t - 4$, and up to 0.5 in the PDV^{NP} mature phase (t); note the focusing of correlations over Micronesia and the Philippine Sea in the mature phase.⁸ Correlations build up in the southeastern equatorial Pacific as well, exceeding 0.4 at $t - 4$ but dissipating prior to the attainment of peak North Pacific amplitudes. Also noteworthy and potentially interesting are the leading correlations (~ 0.4) southeastward of Greenland.

A more in-depth analysis, including modeling, will be necessary to establish the causal significance of the correlated regions in Fig. 12. The Indian Ocean and western tropical Pacific SST links of the PDV^{NP} mode revealed by this analysis are, however, not inconsistent

with the recently highlighted role of the Indian ocean basin (SST, aerosols) in global climate variability: NAO trend (Hoerling et al. 2004), droughts (Lau et al. 2006), monsoon changes/trend (Chung and Ramanathan 2006), and—the one most closely related to this study—Aleutian sector climate variability/shift (Deser and Phillips 2006).

c. Mode physicality

The physicality of the extracted modes is a concern in most statistical analyses, including this one. Could the identified modes be statistical artifacts, for instance? While there is no well-defined strategy to ascertain mode physicality, decadal variations in SST and related physical variables (e.g., precipitation, salinity) can have reflections in the climate-sensitive marine (and terrestrial) ecosystems, including fish recruitment records (Mantua et al. 1997; Chavez et al. 2003),⁹ which can be advantageously used to gauge the physicality of the decadal modes.

Mode physicality is assessed here from correlations of the PDV PCs and the North Pacific and Bering Sea biological time series assembled by Hare and Mantua (2000) for the 1965–97 period. Correlations of the PDO index and biological time series provide a reference point in this assessment. Table 2 lists the three most correlated biological records for each mode: PDV^{PP}, PDV^{NP}, and PDO. The PDO correlations are noted in each case, for reference. The highest annual correlation of the PDV^{PP} mode (0.54) is with the eastern Pacific zooplankton biomass record and then with the British Columbia salmon catches (-0.42)—not surprising, given the coastal focus of the Pan-Pacific mode. The PDV^{NP} mode is most correlated with the Gulf of Alaska halibut record (-0.74), marginally exceeding

⁸ Connections between the tropical/subtropical Indian Ocean and North Pacific SSTs were noted by Kawamura (1994), but Zhang et al. (1996) found the regions weakly connected in the ENSO-filtered fields.

⁹ The ecosystem changes can feed back to the physical climate (e.g., Miller et al. 2003).

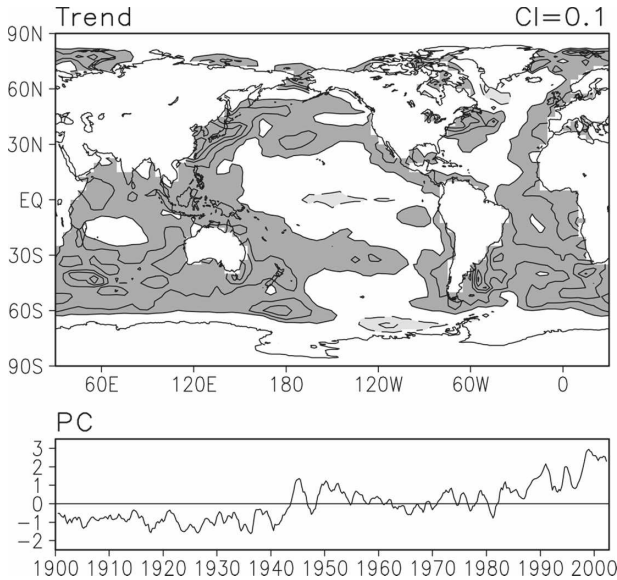


FIG. 13. Secular trend in twentieth-century SSTs based on Pacific basin analysis and consistent with natural SST variability in the same period. Map is generated from SST regressions on the third-leading principal component of the primary analysis (the trend mode, in earlier discussion). Solid (dashed) contours denote positive (negative) values and the zero contour is suppressed. Contour interval is 0.1 K.

the highest PDO correlation (0.73) also with the same recruitment record. The extracted decadal modes, PDV^{PP} and PDV^{NP} , thus appear to be reasonably physical, at least, by this measure. Characterization of variability mechanisms and modeling analysis is, however, needed to rigorously assess the physicality of these modes.

d. Twentieth-century SST trend

The third-leading mode captures the secular trend in the Pacific SST record, as apparent from its PC (Fig. 2), which is strikingly similar to both the global surface air temperature trend [e.g., National Aeronautics and Space Administration Goddard Institute for Space Studies (NASA GISS)] and the ocean heat content

trend (Levitus et al. 2005). Modal structure (Fig. 13) shows pervasive SST warming except for two small regions of cooling in the Northern Hemisphere: an equatorial sliver in the central Pacific and another off the southern tip of Greenland. The warming is evidently largest along the eastern coasts of Asia and North America, where the twentieth-century SST change is as much as 1.5 K. A similar SST pattern emerges from the least squares fitting of the SST trend at each grid point. The displayed EEOF-based extraction and the linear fitted trend (not shown) are spatially correlated at 0.9.

The EEOF-based extraction is preferred, as the secular trend is not constrained to be stationary in time here (which is the case in least squares fitting). It is, moreover, desirable, as noted in the introduction, to extract secular trend in the context of natural variability. The modest fluctuations in PC3 (Fig. 2) as it shifts from negative values in the early century to positive ones in recent decades reflect the accommodation of natural variability.

It is interesting to compare our secular trend with that found in earlier studies. An additional cooling center in the North Pacific is present in Cane et al.'s (1997, their Fig. 3) analysis of linear trend in the 1900–91 Kaplan SSTs (Kaplan et al. 1998). A longer period (1854–1992) analysis by Kaplan et al. (2000) also finds nearly the same. [The additional cooling center must be due to dataset differences, as least squares fitting of the Hadley SST record does not contain this feature.]

5. Sensitivity analysis

Robustness of the spatiotemporal variability modes is ascertained in this section from perturbation of the primary analysis. Table 3 summarizes the sensitivity tests. Each test focuses on an aspect of the primary analysis (T0): analysis domain (T1), climatology base period (T2), analysis period (T3 and T4), number of rotated modes (T5), and sampling window length

TABLE 3. Sensitivity tests: T0 is the primary analysis. The Pacific analysis domain is 20°S–60°N, 120°E–60°W, while the Indo-Pacific one extends it farther westward to 30°E.

Name	Domain	Period	Climatology	Rotated	Time window
T0	Pacific	1900–2002	1900–2002	7	1 season × 5
T1	Indo-Pacific	1900–2002	1900–2002	7	1 season × 5
T2	Pacific	1900–2002	1945–2002	7	1 season × 5
T3	Pacific	1945–2002	1945–2002	7	1 season × 5
T4	Pacific	1900–76	1900–76	7	1 season × 5
T5	Pacific	1900–2002	1900–2002	9	1 season × 5
T6	Pacific	1900–2002	1900–2002	3	2 season × 5
T7	Pacific	1900–2002	1900–2002	3	2 season × 7
T8	Pacific	1900–2002	1900–2002	3	4 season × 5

TABLE 4. Sensitivity test results: column 1 shows the leading modes identified in the primary analysis (T0); numbers following the name indicate the percentage variance explained by the mode and its rank, respectively. Columns 2–9 list attributes of the leading modes in the eight sensitivity tests (T1–T8), with the three-slash numbers indicating correlation between the test case and primary analysis PCs, the percentage variance explained by that mode, and its rank in the test analysis. Asterisks indicate “not applicable.”

T0	T1	T2	T3	T4	T5	T6	T7	T8
ENSO ^{PP} /17.7/1	1.00/16.6/1	1.00/16.6/1	1.00/18.4/1	0.99/18.7/1	0.99/17.2/1	*	*	*
ENSO ^{PM} /13.6/2	1.00/12.8/2	1.00/12.8/3	1.00/14.3/2	0.99/14.7/2	1.00/13.8/2	*	*	*
Trend/10.2/3	0.99/11.4/3	0.99/15.1/2	0.95/6.1/3	0.92/8.3/3	0.98/9.8/3	0.97/16.3/1	0.96/15.9/1	0.90/15.3/1
PDV ^{PP} /5.3/4	0.99/5.0/4	0.99/4.9/4	0.82/4.1/6	0.96/7.8/4	0.77/6.1/4	0.92/6.7/2	0.87/5.8/2	0.78/5.7/3
ENSO ^{NC} /4.3/5	0.98/3.8/6	1.00/4.1/5	0.97/6.0/4	0.69/2.8/7	0.84/3.5/6	*	*	*
PDV ^{NP} /4.3/6	0.98/4.4/5	0.99/4.0/6	0.79/4.7/5	0.77/8.3/3	0.68/3.2/7	0.92/5.9/3	0.87/5.6/3	0.78/5.9/2
Biennial/3.5/7	0.98/3.4/7	1.00/3.3/7	0.98/3.8/7	0.92/3.4/5	0.95/3.5/5	*	*	*

(T6–T8). Tests T1–T5 closely follow the primary analysis (T0), except for the indicated changes. Tests T6–T8 are devised to assess if the five-season-long sampling window is of sufficient duration to sample decadal variability, and these are, of necessity, implemented somewhat differently. In these, SST is first residually reconstructed from the primary analysis PCs and EOFs [i.e., by excluding ENSO (ENSO⁻, ENSO⁺, ENSO^{NC}) and the biennial modes from the raw anomalies]. The reconstructed SSTs are then analyzed with longer sampling windows (14–20-season duration), but with rotation of three modes in the interest of comparison with the primary analysis.

Table 4 summarizes the test findings by tabulating the mode order, percentage of explained variance, and correlation between the T0 and test case PCs. Of these, correlations is perhaps most indicative of analysis stability. Table 4 suggests

- robust stability of the ENSO⁻, ENSO⁺, biennial, and trend modes; correlations in the 0.92–1.0 range;
- that analysis period differences (T3, T4) impact the low-frequency modes, not surprisingly. ENSO^{NC} is impacted most (0.69–0.97) because of its uneven energy in the record, more in the second half (cf. Fig. 2), consistent with its accounting of more variance in T3 than in T0 or T4;
- lack of separation between the trend and PDV^{NP} mode in the pre-climate shift period, for the third mode in T4 is correlated to both the trend (0.92) and PDV^{NP} (0.77) modes of T0. This lack of separation is also suggested by their similar PC structure in this period in Fig. 2;

TABLE 5. Number of “analogs” in five EOF analyses of 1900–2002 Pacific SST variability. See text for details, including analog definition.

EOF	Rotated EOF	EEOF	Rotated EEOF (7 rotated)	Rotated EEOF (9 rotated)
46	56	37	46	37

- insensitivity of the PDV modes to sampling window variations (T6–T8), indicating sufficiency of the five-season sampling window of the primary analysis for detection and separation of biennial, ENSO, and decadal variabilities, and secular trend, all in one step.

A lingering concern in EOF analysis pertains to rotation—not just the number of modes rotated (investigated above) but to rotation itself: Does rotation of EOFs yield more “physical” modes of variability? A physical realization of the extracted modes would, surely, be the ultimate proof of physicality, but it is seldom that variations from climatology are composed of just one mode of variability in nature (i.e., with all other modes suppressed at the same time). Of course, when this happens, an observational “analog” of that mode is encountered. The number of observational analogs of an extracted set of modes in the record can be one objective measure of the “physicality” of that extraction, and this strategy is used here.

An observed anomaly will be deemed a modal analog in the context of an extraction, should any one PC be larger than all others in that analysis by at least one unit of magnitude; note, PCs are orthonormal with or without rotation. The identification is objective and easily implemented, and Table 5 presents the number of analogs found in five analyses. The number is expectedly small, as analogs are rare: ~10% in Table 5 as 408 anomalies (five-season span) are analyzed in each case. A significant increase (~20%) in the number of analogs in the corresponding rotated analysis (regular or extended) is noted. Interestingly, rotating nine modes reduces the number of analogs, further justifying our choice of rotating seven modes in the primary EEOF analysis.

6. Synopsis and concluding remarks

The twentieth-century SSTs in the Pacific basin are analyzed for consistent characterization of natural variability and secular trend, motivated by the need to ap-

portion oceanic warming, both temporally and regionally. The evolution-centric analysis is conducted using the extended EOF technique, which was introduced to climate sciences by Weare and Nasstrom (1982) almost a quarter-century ago, and interestingly, demonstrated on Pacific SSTs!

The technique is effective in separating variability modes having similar spatial patterns but different temporal evolution and/or time scales. Pacific decadal variability, which is reckoned to include an “ENSO-like” structure, would thus be a choice test problem. But for reasons unknown, PDV characterization has hitherto been undertaken with temporally filtered datasets, when filtering can inadvertently alias the target structures; data detrending can, likewise, be problematic. Many of these concerns become moot with extended EOF analysis. The method is particularly effective in characterizing both the nascent and mature phases of variability.

Findings from a *single* analysis that effectively discriminates between biennial, ENSO, and decadal variabilities, and between these natural variability modes and the secular trend, are reported in this study. The principal findings are

- *canonical ENSO variability*: encapsulated in two modes that depict the growth (east to west along the equator; ENSO⁻) and decay (near-simultaneous amplitude loss across the basin; ENSO⁺) phases; ENSO⁺ lags ENSO⁻ by three seasons, and the Niño-3.4 SST index by one season;
- *noncanonical ENSO variability*: represented by an interannual mode of comparatively lower frequency that has been energetic in recent decades; shown linked to the west-to-east SST development seen in post-climate shift ENSOs; the ENSO^{NC} mode. It leads the Niño-3.4 index by five seasons in the recent record. The ENSO^{NC} mode is closely related to Chiang and Vimont’s (2004) meridional mode, which represents interannual-to-decadal variability in the tropical basin, much as in here;
- *ENSO time scale*: autocorrelation of synthetic Niño-3.4 SST indices shows that the ENSO^{NC} mode leads to some reduction in canonical ENSO’s oscillatory tendency, while the addition of the biennial mode reduces the duration of canonical episodes, by ~0.5 yr;
- *Niño-3.4 SST index*: composed of canonical, noncanonical, and biennial variability. Original index correlated with the synthetic one based on canonical modes at 0.84, with the canonical- plus noncanonical-based synthetic index at 0.93 and with the index that additionally includes the biennial mode at 0.95;

- *Pacific decadal SST variability*: characterized by two modes:
 - the *Pan-Pacific* mode (PDV^{PP}) has a horseshoe-shaped structure with the closed end skirting the North American coast, and a quiescent central/eastern equatorial Pacific. Surprising connections to the tropical/subtropical Atlantic (Caribbean correlations 0.4–0.5), with structure resembling the Atlantic multidecadal oscillation; AMO and PDV^{PP} are correlated at 0.42, and at 0.48 at five-season PDV^{PP} lead. Reference to this mode as ENSO like is misleading in our opinion.
 - the *North Pacific* mode (PDV^{NP}) has a zonal band of SST anomalies extending eastward from Japan as its principal feature. The mode captures the 1976/77 climate shift and exhibits some correspondence to Mantua’s Pacific decadal oscillation (correlation 0.57). The present analysis shows, perhaps for the first time, the striking links of the North Pacific mode to the western tropical Pacific and Indian Ocean SSTs. Links to the region southeast of Greenland are also noteworthy.
- *mode physicality*: physicality of decadal modes (whose long time scales potentially permit marine population adjustments) is assessed from correlations with biological time series in the North Pacific (from Hare and Mantua 2000). The reported extractions evidently fare at least as well as the PDO index (cf. Table 2);
- *twentieth-century secular trend*: implicit accommodation of natural variability leads to a nonstationary SST trend, including midcentury cooling. The SST trend is remarkably similar to the global surface air temperature and ocean heat content trends. Geographically, a sliver of cooling in the central equatorial Pacific is seen in the midst of widespread but nonuniform warming. Intercomparison shows that linear trend overestimates warming near the Aleutians and along the North American coast, and also in the tropical Indian and Atlantic basins.

The study provides a basis for

- investigation of the origin and mechanisms of Pacific decadal variability. The finding of connections with the adjoining tropical basins provides interesting leads, as does analysis of the subsurface structure (upper-ocean heat content in particular) (e.g., Xie et al. 2000; Schneider and Cornuelle 2005). An Estimating the Circulation and Climate of the Ocean (ECCO)-based (Koehl et al. 2006) analysis is planned;
- assessment of climate system models, from analysis of SST variability in Intergovernmental Panel on Climate Change (IPCC) simulations of the twentieth-

century climate, where greenhouse gas loadings have the same trend as in nature;

- refining estimates of regional climate/hydroclimate change, from analysis of the nonstationary secular trend and linear trend regressions, especially their differences;
- advancing understanding of the mediating role of oceans in climate change: similarity of the SST (ocean heat content) and surface air temperature trends must imply oceanic control. But why then is the mid-century cooling attributed to aerosols present in near-real time in the ocean surface and subsurface records? What about ocean thermal inertia?

Acknowledgments. The authors thank their colleague, Alfredo Ruiz-Barradas, for expert help with datasets and analysis in the initial phase of the study. We thank Nate Mantua for advice and pointers on marine biological records, and Dan Vimont for helpful clarifying discussions.

Bin Guan and Sumant Nigam acknowledge support of Grants NOAA/CPPA NA17EC1483 and NSF ATM-0649666.

REFERENCES

- Barlow, M., S. Nigam, and E. H. Berbery, 2001: ENSO, Pacific decadal variability, and U.S. summertime precipitation, drought, and stream flow. *J. Climate*, **14**, 2105–2127.
- Barnett, T. P., 1991: The interaction of multiple timescales in the tropical climate system. *J. Climate*, **4**, 269–285.
- Cane, M. A., A. C. Clement, A. Kaplan, Y. Kushnir, D. Pozdnyakov, R. Seager, S. E. Zebiak, and R. Murtugudde, 1997: Twentieth-century sea surface temperature trends. *Science*, **275**, 957–960.
- Carton, J. A., and B. Huang, 1994: Warm events in the tropical Atlantic. *J. Phys. Oceanogr.*, **24**, 888–903.
- Cattell, R. B., 1966: The scree test for the number of factors. *J. Multiv. Behav. Res.*, **1**, 245–276.
- Chavez, F. P., J. Ryan, S. E. Lluch-Cota, and M. Niquen C., 2003: From anchovies to sardines and back: Multidecadal change in the Pacific Ocean. *Science*, **299**, 217–221.
- Chiang, J. C. H., and D. J. Vimont, 2004: Analogous Pacific and Atlantic meridional modes of tropical atmosphere–ocean variability. *J. Climate*, **17**, 4143–4158.
- Chung, C., and S. Nigam, 1999: Weighting of geophysical data in principal component analysis. *J. Geophys. Res.*, **104**, 16 925–16 928.
- , and V. Ramanathan, 2006: Weakening of North Indian SST gradients and the monsoon rainfall in India and the Sahel. *J. Climate*, **19**, 2036–2045.
- Deser, C., and J. M. Wallace, 1990: Large-scale atmospheric circulation features of warm and cold episodes in the tropical Pacific. *J. Climate*, **3**, 1254–1281.
- , and M. L. Blackmon, 1995: On the relationship between tropical and North Pacific sea surface temperature variations. *J. Climate*, **8**, 1677–1680.
- , and A. S. Phillips, 2006: Simulation of the 1976/77 climate transition over the North Pacific: Sensitivity to tropical forcing. *J. Climate*, **19**, 6170–6180.
- Enfield, D. B., A. M. Mestas-Nuñez, and P. J. Trimble, 2001: The Atlantic multidecadal oscillation and its relation to rainfall and river flows in the continental U.S. *Geophys. Res. Lett.*, **28**, 2077–2080.
- Graham, N. E., 1994: Decadal-scale climate variability in the tropical and North Pacific during the 1970s and 1980s: Observations and model results. *Climate Dyn.*, **10**, 135–162.
- Gu, D., and S. G. H. Philander, 1995: Secular changes of annual and interannual variability in the tropics during the past century. *J. Climate*, **8**, 864–876.
- Hare, S. R., and N. J. Mantua, 2000: Empirical evidence for North Pacific regime shifts in 1977 and 1989. *Prog. Oceanogr.*, **47**, 103–145.
- Hoerling, M. P., J. W. Hurrell, T. Xu, G. T. Bates, and A. S. Phillips, 2004: Twentieth century North Atlantic climate change. Part II: Understanding the effect of Indian Ocean warming. *Climate Dyn.*, **23**, 391–405.
- Kalnay, E., and Coauthors, 1996: The NCEP/NCAR 40-Year Reanalysis Project. *Bull. Amer. Meteor. Soc.*, **77**, 437–471.
- Kaplan, A., M. A. Cane, Y. Kushnir, A. C. Clement, M. B. Blumenthal, and B. Rajagopalan, 1998: Analysis of global sea surface temperatures 1856–1991. *J. Geophys. Res.*, **103**, 18 567–18 589.
- , Y. Kushnir, and M. A. Cane, 2000: Reduced space optimal interpolation of historical marine sea level pressure: 1854–1992. *J. Climate*, **13**, 2987–3002.
- Kawamura, R., 1994: A rotated EOF analysis of global sea surface temperature variability with interannual and interdecadal scales. *J. Phys. Oceanogr.*, **24**, 707–715.
- Koehl, A., D. Dommenges, K. Ueyoshi, and D. Stammer, 2006: The Global ECCO 1952 to 2001. Ocean Synthesis Rep. 40, 43 pp.
- Lau, K. M., S. S. P. Shen, K.-M. Kim, and H. Wang, 2006: A multimodel study of the twentieth-century simulations of Sahel drought from the 1970s to 1990s. *J. Geophys. Res.*, **111**, D07111, doi:10.1029/2005JD006281.
- Levitus, S., J. Antonov, and T. Boyer, 2005: Warming of the world ocean, 1955–2003. *Geophys. Res. Lett.*, **32**, L02604, doi:10.1029/2004GL021592.
- Mantua, N. J., S. R. Hare, Y. Zhang, J. M. Wallace, and R. C. Francis, 1997: A Pacific interdecadal climate oscillation with impacts on salmon production. *Bull. Amer. Meteor. Soc.*, **78**, 1069–1079.
- Mestas-Nuñez, A. M., and D. B. Enfield, 1999: Rotated global modes of non-ENSO sea surface temperature variability. *J. Climate*, **12**, 2734–2746.
- , and —, 2001: Eastern equatorial Pacific SST variability: ENSO and non-ENSO components and their climatic associations. *J. Climate*, **14**, 391–402.
- Miller, A. J., and Coauthors, 2003: Potential feedbacks between Pacific Ocean ecosystems and interdecadal climate variations. *Bull. Amer. Meteor. Soc.*, **84**, 617–633.
- Minobe, S., 1997: A 50–70 year climatic oscillation over the North Pacific and North America. *Geophys. Res. Lett.*, **24**, 683–686.
- Monahan, A. H., 2001: Nonlinear principal component analysis: Tropical Indo–Pacific sea surface temperature and sea level pressure. *J. Climate*, **14**, 219–233.
- Nakamura, H., G. Lin, and T. Yamagata, 1997: Decadal climate variability in the North Pacific during the recent decades. *Bull. Amer. Meteor. Soc.*, **78**, 2215–2225.
- Nigam, S., and H.-S. Shen, 1993: Structure of oceanic and atmo-

- spheric low-frequency variability over the tropical Pacific and Indian Oceans. Part I: COADS observations. *J. Climate*, **6**, 657–676.
- , M. Barlow, and E. H. Berbery, 1999: Analysis links Pacific decadal variability to drought and streamflow in United States. *Eos, Trans. Amer. Geophys. Union*, **80**, 621–625.
- Nitta, T., and S. Yamada, 1989: Recent warming of tropical sea surface temperature and its relationship to the Northern Hemisphere circulation. *J. Meteor. Soc. Japan*, **67**, 375–383.
- Overland, J. E., and R. W. Priesendorfer, 1982: A significance test for principal components applied to a cyclone climatology. *Mon. Wea. Rev.*, **110**, 1–4.
- Rasmusson, E. M., and T. H. Carpenter, 1982: Variations in tropical sea surface temperature and surface wind fields associated with the Southern Oscillation/El Niño. *Mon. Wea. Rev.*, **110**, 354–384.
- , X. Liang, and C. F. Ropelewski, 1990: The biennial component of ENSO variability. *J. Mar. Syst.*, **1**, 71–96.
- Rayner, N. A., D. E. Parker, E. B. Horton, C. K. Folland, L. V. Alexander, D. P. Rowell, E. C. Kent, and A. Kaplan, 2003: Global analyses of sea surface temperature, sea ice, and night marine air temperature since the late nineteenth century. *J. Geophys. Res.*, **108**, 4407, doi:10.1029/2002JD002670.
- Richman, M. B., 1986: Rotation of principal components. *Int. J. Climatol.*, **6**, 293–335.
- Schneider, N., and B. D. Cornuelle, 2005: The forcing of the Pacific decadal oscillation. *J. Climate*, **18**, 4355–4373.
- Schubert, S. D., M. J. Suarez, P. J. Pegion, R. D. Koster, and J. T. Bacmeister, 2004: On the cause of the 1930s Dust Bowl. *Science*, **303**, 1855–1859.
- Seager, R., Y. Kushnir, C. Herweijer, N. Naik, and J. Velez, 2005: Modeling of tropical forcing of persistent droughts and pluvials over western North America: 1856–2000. *J. Climate*, **18**, 4065–4088.
- Ting, M., and H. Wang, 1997: Summertime U.S. precipitation variability and its relation to Pacific sea surface temperature. *J. Climate*, **10**, 1853–1873.
- Trenberth, K. E., 1990: Recent observed interdecadal climate changes in the Northern Hemisphere. *Bull. Amer. Meteor. Soc.*, **71**, 988–993.
- , and D. P. Stepaniak, 2001: Indices of El Niño evolution. *J. Climate*, **14**, 1697–1701.
- von Storch, H., and F. W. Zwiers, 1999: *Statistical Analysis in Climate Research*. Cambridge University Press, 494 pp.
- Wang, B., 1995: Interdecadal changes in El Niño onset in the last four decades. *J. Climate*, **8**, 267–285.
- Weare, B. C., and J. S. Nasstrom, 1982: Examples of extended empirical orthogonal function analyses. *Mon. Wea. Rev.*, **110**, 481–485.
- Wu, L., Z. Liu, R. Gallimore, R. Jacob, D. Lee, and Y. Zhong, 2003: Pacific decadal variability: The tropical Pacific mode and the North Pacific mode. *J. Climate*, **16**, 1101–1120.
- Xie, S.-P., T. Kunitani, A. Kubokawa, M. Nonaka, and S. Hosoda, 2000: Interdecadal thermocline variability in the North Pacific for 1958–1997: A GCM simulation. *J. Phys. Oceanogr.*, **30**, 2798–2813.
- Zhang, R.-H., and A. J. Busalacchi, 2005: Interdecadal change in properties of El Niño–Southern Oscillation in an intermediate coupled model. *J. Climate*, **18**, 1369–1380.
- Zhang, Y., J. M. Wallace, and N. Iwasaka, 1996: Is climate variability over the North Pacific a linear response to ENSO? *J. Climate*, **9**, 1468–1478.
- , —, and D. S. Battisti, 1997: ENSO-like interdecadal variability: 1900–93. *J. Climate*, **10**, 1004–1020.

Copyright of *Journal of Climate* is the property of *American Meteorological Society* and its content may not be copied or emailed to multiple sites or posted to a listserv without the copyright holder's express written permission. However, users may print, download, or email articles for individual use.